

# Nanoscale Electroviscous Lift Force

Hao Zhang,<sup>1, 2,\*</sup> Zaicheng Zhang,<sup>3,\*</sup> Thomas Guérin,<sup>2</sup> and Abdelhamid Maali<sup>2, †</sup>

<sup>1</sup>*State Key Laboratory of Structural Chemistry, Fujian Institute of Research on the Structure of Matter, Chinese Academy of Sciences, Fuzhou 350002, China*

<sup>2</sup>*Laboratoire Ondes et Matière d'Aquitaine, CNRS/University of Bordeaux, F-33400 Talence, France*

<sup>3</sup>*School of Physics, Beihang University, 100191 Beijing, China*

About forty years ago, it has been predicted that a charged particle, moving parallel to a charged wall in an electrolyte, should experience a lift force that, contrarily to electrostatic forces, is not screened at large distances. Up to now, such electroviscous lift force has not been directly measured. Here, we use Atomic Force Microscopy to directly measure the electroviscous lift force and quantify its dependency with the distance to the wall, the translation velocity or the particle's size. Observing that existing theories exhibit large discrepancies with our experimental observations, we develop an analytical approach combining lubrication theory to a previously introduced formalism for small screening length. The experimentally observed lift forces are in good agreement with our theoretical predictions and reveal, for the first time, a saturation of the lift force for increasing velocities. Altogether, our results characterize, through direct measurements and analytical approach, the properties of electroviscous forces between charged particles in viscous electrolytes in non-equilibrium conditions.

Electrolyte flows in confined geometries or near charged surfaces are fundamentally affected by the presence of electric double layers (EDLs) that form at the interfaces [1–4]. Hydrodynamic flows disturb the ionic clouds next to the charged surfaces, resulting in the distortion of the EDL and inducing a dynamic coupling between viscous flow and charge distribution, giving rise to a range of electroviscous effects. These include ion transport in nanofluidic channels driven by surface charge [5], reduction of diffusion of colloids near charged boundaries [6, 7], increased shear viscosity in charged colloidal suspensions [8, 9], and enhanced drag forces on charged particles moving near walls [10–14].

About four decades ago, Prieve and co-workers [15–18] proposed an electro-hydrodynamic mechanism for lubrication in electrolytes. Their theoretical calculations showed that for a charged sphere sliding near a charged surface, the flow-induced distortion of ion distributions generates Maxwell stresses, producing a repulsive electrokinetic lift force. While electrostatic forces are screened in electrolytes, this dynamic force, arising from electrohydrodynamic coupling, persists and decays algebraically with the distance to the surface. The calculated lift force increases with sliding velocity and fluid viscosity, but diminishes with increasing ionic strength. Notably, this force acts to prevent mechanical contact between surfaces, suggesting a novel mode of electric lubrication in charged wet matter systems. It is worth noting that for a neutral rigid sphere moving over a neutral rigid substrate at low Reynolds numbers, the normal stress (pressure field) is antisymmetric: it is positive at the front and negative at the rear, resulting in a zero net normal force. In the electro-hydrodynamic mechanism [15–18] however, the sphere and substrate are charged and im-

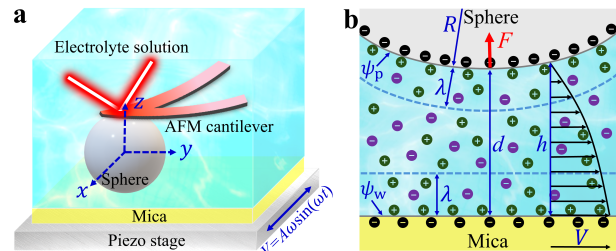


FIG. 1. Schematic illustration of the experimental setup used to measure the electroviscous lift force acting on a charged sphere moving along a charged rigid surface in an electrolyte environment. A borosilicate glass sphere is fixed to the tip of an AFM cantilever, which acts as a force sensor. The mica substrate, immersed in electrolyte solution, is mounted on a piezoelectric stage that imposes controlled lateral oscillations. The resulting force acting on the sphere, is obtained from the measurements of the cantilever vertical deflection.

mersed in an electrolyte. The normal stress includes a Maxwell stress contribution that breaks this antisymmetry and generates a finite lift force. This situation is analogous to the emergent lift forces that were recently observed for spheres or cylinders moving past soft interfaces, where elastohydrodynamic effects similarly disrupt the antisymmetry of the normal stress [19–24].

Subsequent theoretical work [25–27] incorporated the role of hydrodynamic stresses and explicitly formulated the electroviscous formalism for gap distances larger than the Debye layer thickness. Explicit predictions were obtained for spheres or cylinders moving next to a plane wall [28–31], in the limit of small velocities.

Despite this theoretical progress, experimental evidence for electro-viscous lift remains limited. To date, all measurements of the electro-viscous lift force have been indirect, either by tracking particle heights under shear in the presence of gravity [15, 32, 33] or by inferring forces through evanescent wave particle tracking in combined

\* These authors contributed equally to this work.

† [abdelhamid.maali@u-bordeaux.fr](mailto:abdelhamid.maali@u-bordeaux.fr)

electroosmotic and pressure-driven flows [34]. The absence of direct measurements of this electro-viscous lift force highlights the experimental challenges in resolving weak, velocity-dependent normal forces at nanoscales. The colloidal atomic force microscopy (AFM) probe has proven to be a powerful tool for measuring weak forces [35, 36]. Recently, this technique was successfully used to probe the emergent lift force acting on spherical particles moving along soft interfaces [22, 23]. This method requires only accurate calibration of the AFM cantilever.

In this work, we report the direct and quantitative measurements of the electroviscous lift force acting on a spherical particle moving along a planar wall in electrolyte solutions. Using AFM, the lift force is measured as a function of the separation distance. Experiments were conducted at different sliding velocities and with particles of varying radii. The obtained experimental results cannot be explained by existing theories. We thus develop an analytical approach, derived using Cox's formalism in the lubrication regime. Our theory quantitatively matches with observed lift forces and reveals a previously overlooked saturation of the force for high velocities.

A sketch of the experimental configuration is shown in Fig. 1. The experiment was performed using an AFM (Dimension 3100, Bruker) equipped with a liquid cell (DTFML-DD-HE). Borosilicate glass spheres (MO-Sci Corporation) with radii of  $R = 56.6 \pm 0.2 \mu\text{m}$  and  $R = 24.4 \pm 0.2 \mu\text{m}$  were glued to the ends of two AFM cantilevers (SNL-10, Bruker Probes). The stiffness of the cantilevers attached with spheres are calibrated using a hydrodynamic drainage method [37], yielding values of  $k_c = 0.40 \pm 0.02 \text{ N/m}$  and  $k_c = 0.27 \pm 0.02 \text{ N/m}$ , respectively. The mica substrate was fixed on a piezo stage (E-709.CHG, PI), which enabled lateral oscillations at angular frequencies  $\omega$  ranging from 126 to 503  $\text{s}^{-1}$ , with amplitudes  $A$  between 7.2 and 17.1  $\mu\text{m}$ . The imposed velocity is  $V(t) = V_0 \cos(\omega t)$ , with probed velocity amplitudes  $V_0 = A\omega$  ranging between 1.3 and 8.1  $\text{mm/s}$ . The Debye length, which sets the characteristic range of electrostatic interactions, is inversely proportional to square root of the ionic strength. The electrolyte solution used in all experiments was deionized water containing 0.1 mM NaCl. This salt concentration was chosen so that electric effects are dominated by  $\text{Na}^+$  and  $\text{Cl}^-$  ions (and not by carbonate ions due to the dissolution of  $\text{CO}_2$ ), while at the same time maintaining a sufficiently long Debye length to enable the measurements of electric interactions.

To determine the electric potential at the surface of the wall ( $\psi_w$ ) and of the spherical particle ( $\psi_p$ ), we first measure the double layer (DL) force in static conditions (Fig. 2a), whose theoretical expression reads [38]:

$$F_{\text{DL}} = \frac{64\epsilon\pi R}{\lambda} \left( \frac{k_B T}{e} \right)^2 \tanh \frac{e\psi_p}{k_B T} \tanh \frac{e\psi_w}{k_B T} e^{-d/\lambda}, \quad (1)$$

where the minimal distance  $d$  between the particle and the wall is assumed to be larger than the Debye length

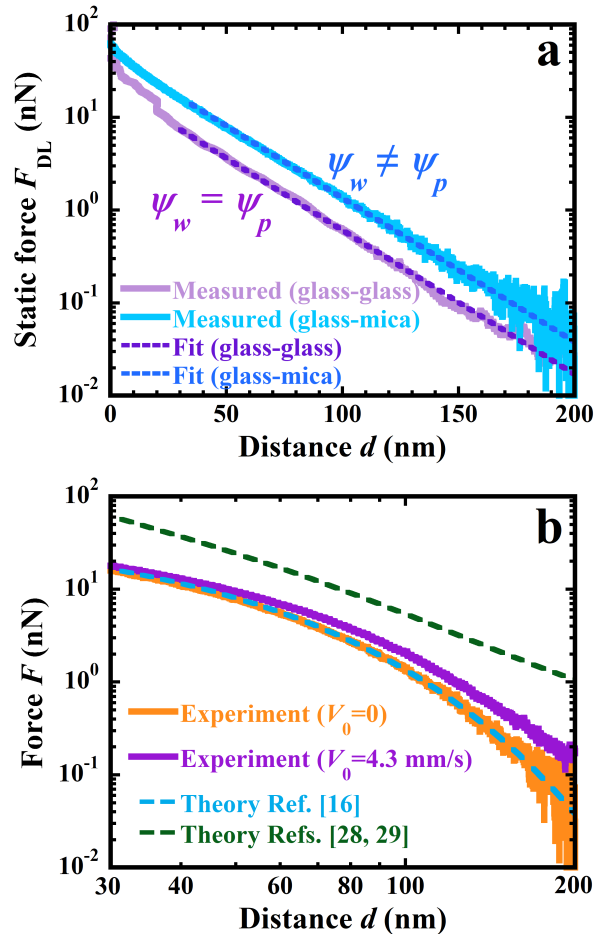


FIG. 2. (a) Measured static force between a borosilicate glass sphere (radius:  $56.6 \mu\text{m}$ ) and either a borosilicate glass substrate or a mica substrate in 0.1 mM NaCl solution under static conditions (zero velocity). Dashed lines represent theoretical fits from Eq. (1). From the fitting results, we obtain  $\lambda = 28 \text{ nm}$ ,  $\psi_p = -36 \pm 3 \text{ mV}$ , and  $\psi_w = -100 \pm 5 \text{ mV}$ . Note that the contribution of van der Waals forces is neglected, since here it is negligible at distances larger than the Debye length. (b) Log-log plot of the measured double-layer force (orange) and total time averaged force (purple, sum of the double-layer and electro-viscous lift forces), obtained with a  $56.6 \mu\text{m}$ -radius sphere oscillating at a velocity amplitude of  $V_0 = 4.3 \text{ mm/s}$ . For comparison, total forces, as the sum of the static force Eq. (1) and the lift forces predicted by Prieve and co-workers [16] [Eq. (S9) in SI] or Warszynski *et al.* [28, 29] [Eq. (S10) in SI], taking into account that  $\langle V^2 \rangle = V_0^2/2$ , are also shown.

$\lambda = \sqrt{\epsilon k_B T / (2e^2 c_\infty)}$ , with  $\epsilon$  the liquid's permittivity,  $k_B T$  the thermal energy,  $e$  the elementary charge and  $c_\infty$  the bulk ionic concentration.

First, we replace the planar mica surface by the borosilicate glass that forms the spherical particle and fit the measured static force with Eq. (1) assuming  $\psi_w = \psi_p$ , yielding a surface potential of  $\psi_p = -36 \pm 3 \text{ mV}$  for the borosilicate sphere. Once this value was determined, the surface potential of the mica substrate was obtained

by measuring the static force between the borosilicate sphere and the mica surface in the same solution, yielding  $\psi_w = -100 \pm 5$  mV.

Figure 2b shows the measured force as a function of the gap distance between the glass sphere and the mica surface. The force was measured for a lateral velocity amplitude of  $V_0 = 4.3$  mm/s, and the static double-layer force, obtained without applying lateral motion, is also shown for comparison. At small separations, the two forces nearly coincide; however, at larger distances, the force measured during substrate motion exceeds that of the static case. This observation provides direct evidence of the electro-viscous lift force, which repels the sphere from the moving surface. Hereafter, we define the lift force  $F_{\text{lift}} \equiv F - F_{\text{DL}}$  as the difference between the total force  $F$  and the static double layer force  $F_{\text{DL}}$ .

On the same graph, we represent existing predictions for this lift force available for the sphere wall geometry. The first one is the theory of Prieve and co-workers [15, 18] [see Eq. (S9) in SI], where the lift force arises from the Maxwell stress associated to the electric field generated by the hydrodynamic flow imposed by the bead's lateral motion, in the lubrication approximation. As can be seen in Fig. 2b, this force cannot explain the increase of the total force induced by the lateral oscillation of the sphere. This may not be surprising since it was already pointed out [25] that the electric field induced by the hydrodynamic flow generates an additional flow, associated to a viscous stress tensor that dominates over the Maxwell electric stress. A second prediction is that of Refs. [28, 29] [see Eq. (S10) in SI], where the general formalism of Cox [25] was applied to the cylinder-wall geometry in the lubrication regime and generalized to the sphere-wall geometry using Derjaguin's approximation. As observed in Fig. 2b, this lift force cannot explain the experimental data since it is about one order of magnitude larger than the experimentally observed lift force. Another prediction for the sphere-wall geometry, obtained [30], is not represented in Fig. 2b since for our parameters it predicts an attractive lift force.

We now present a theoretical analysis of the problem, in the case that the sphere is fixed and the wall moves at constant velocity  $V$ . The equations to be solved are the transport equation for the diffusion of ions in the presence of hydrodynamic flow and electric field, the Poisson equation for the electric potential generated by the ions, and the Stokes equation for the flow (which also depends on the concentration of ions). Since all phenomena (ion transport - flow - electric field) are coupled in non-linear ways, this is a challenging theoretical problem. When the distance between the particle and the wall is large compared to the screening length  $\lambda$ , analytical progress can be made by using matched asymptotic expansion, separating the medium into inner layers (at distances of the order of the Debye length from the walls) and an outer region (far from the walls), where electroneutrality is achieved, but where effective boundary conditions describing the exchange of ions with the double layer. This

was done by Cox. [25]. Here, we analyze these equations by adapting the standard lubrication approach. Clearly,  $d$  is the relevant lengthscale for the vertical direction, while in the lateral directions the relevant lengthscale is  $l = \sqrt{Rd}$ , since the local height can be written as  $H = h/d = 1 + (X^2 + Y^2)/2$ , where  $X = x/l$  and  $Y = y/l$  are rescaled horizontal coordinates. A relevant parameter is the Peclet number  $\text{Pe} = Vl/D_e$  associated to this lengthscale  $l$ , where  $D_e = 2D_+D_-/(D_+ + D_-)$  is the effective diffusion coefficient of ions. Here,  $D_+$  and  $D_-$  are the respective diffusivities of cations and anions, which for NaCl read  $D_+ = 1.33 \times 10^{-9}$  m<sup>2</sup>/s and  $D_- = 2.03 \times 10^{-9}$  m<sup>2</sup>/s.

We first consider the concentration of cations  $c$  at distances larger than the Debye length from the interfaces. Since electroneutrality holds in this outer region,  $c$  is also the concentration of anions. Applying the lubrication approach to Cox equations, we find an effective two-dimensional advection diffusion equation for the rescaled concentration  $N = (c - c_\infty)d^2/(c_\infty\lambda^2)$  that reads (see SI for details)

$$\text{Pe} \bar{\mathbf{U}}_\parallel \cdot \nabla_\parallel N = \nabla_\parallel \cdot (H \nabla_\parallel N) + 2\text{Pe}(\alpha_w S_\perp^w + \alpha_p S_\perp^p), \quad (2)$$

where  $\nabla_\parallel = \hat{\mathbf{e}}_x \partial_X + \hat{\mathbf{e}}_y \partial_Y$ ,  $\bar{\mathbf{U}}_\parallel$  is the dimensionless flow integrated over the vertical coordinate, and the dimensionless parameters  $\alpha_s$  are defined by

$$\alpha_s = \frac{\psi_s e D_+ - D_-}{k_B T D_+ + D_-} + 4 \ln \cosh \frac{\psi_s e}{4k_B T}, \quad s \in \{w, p\}. \quad (3)$$

Finally, the source term  $S_\perp^s = \frac{d}{2V} \partial_n^2(\mathbf{u} \cdot \mathbf{n})$  is proportional to the normal component of the flow to the surface  $s$  and represents the exchange of ions with the Debye layer. Here,  $\partial_n = \mathbf{n} \cdot \nabla$  and  $\mathbf{n}$  denotes the normal to the surface, pointing towards the liquid. Importantly, the effective flow and source terms can be derived explicitly using the known value of the flow induced by the lateral motion of the bead [39], leading to

$$\bar{\mathbf{U}}_\parallel = \left( \frac{3}{5} + \frac{X^2 + 3Y^2}{10} \right) \hat{\mathbf{e}}_x - \frac{XY}{5} \hat{\mathbf{e}}_y, \quad (4)$$

$$S_\perp^s = \frac{1}{10H^3} \times \begin{cases} X(26 + X^2 + Y^2) & (s = p) \\ 4X(4 - X^2 - Y^2) & (s = w) \end{cases}. \quad (5)$$

Next, Cox theory takes into account the flow that is generated by the non-equilibrium concentration of ions, the lift force is dominated by the associated viscous stress. We show in the SI that, in the lubrication regime for a sphere wall geometry, this force can be integrated and reads

$$F_{\text{lift}} = F_0 \Phi(\text{Pe}, \alpha_p, \alpha_w), \quad F_0 = \epsilon \left( \frac{k_B T \lambda}{e} \right)^2 \frac{R}{d^3}, \quad (6)$$

where  $F_0$  is a characteristic force and the dimensionless lift force  $\Phi$ , depending only on the Peclet number and

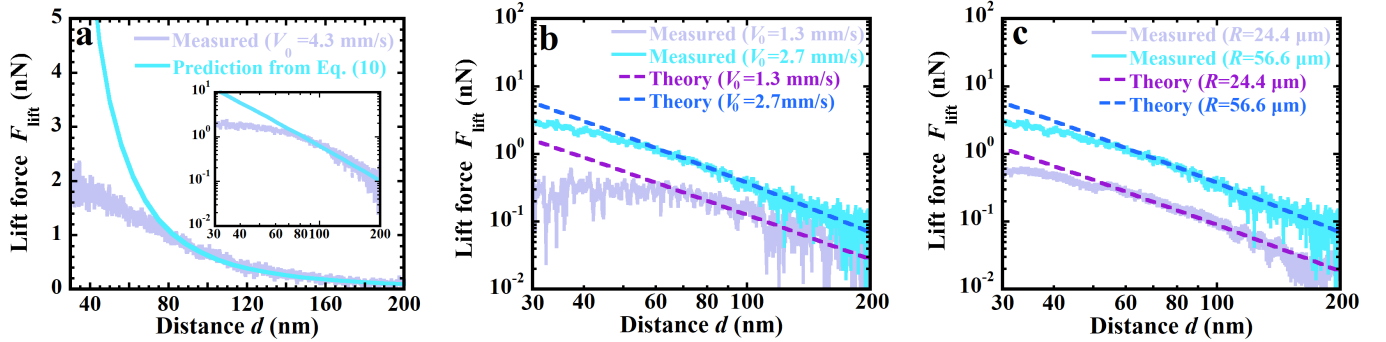


FIG. 3. (a) Lift force ( $F_{\text{lift}}$ ), obtained by subtracting the static double-layer force ( $F_{\text{DL}}$ , measured at zero velocity) from the total force ( $F$ ) measured during lateral oscillations, for a velocity of  $V_0 = 4.3 \text{ mm/s}$  and a sphere radius  $R = 56.6 \mu\text{m}$ , as a function of separation distance  $d$ . The continuous light blue line represents the prediction of Eq. (10). Inset: same data on a logarithmic scale. (b) Lift forces measured at two velocities, 1.3 mm/s and 2.7 mm/s, with a sphere radius of  $R = 56.6 \mu\text{m}$ . Dash-dotted lines are the theoretical predictions. (c) Measurements performed with spheres of radii 56.6  $\mu\text{m}$  and 24.4  $\mu\text{m}$  at  $V_0 = 2.7 \text{ mm/s}$ .

the parameters  $\alpha_w, \alpha_p$ , reads

$$\Phi = 3(\alpha_p + \alpha_w) \iint_{\mathcal{R}^2} dXdY \frac{\nabla \cdot N \cdot \nabla \cdot H}{H^2}. \quad (7)$$

As seen in the above equation, the force is generated by the ionic concentration gradients. Note that the equation for the electric field in the lubrication approximation can be derived but is irrelevant since it does not contribute to the force. For a fixed value of the Peclet, it is straightforward to integrate the two-dimensional partial differential equations (2), (4), and (5) for  $N$ , leading to the determination of  $\Phi$ . Our theory is valid in the regime  $\lambda \ll d \ll R$ .

Analytical calculations can be performed in the small and large Peclet limits, respectively. For small Peclet, we find that  $\Phi \sim \text{Pe}^2$ , determining the coefficients leads to

$$F_{\text{lift}} \underset{\text{Pe} \ll 1}{\simeq} \epsilon \left( \frac{k_B T \lambda V R}{e D_e d} \right)^2 (\alpha_p + \alpha_w) \left[ \frac{6\pi}{25} (\alpha_w + \alpha_p) + k(\alpha_p - \alpha_w) \right] \quad (8)$$

with  $k \simeq 0.49$ . In this regime, the force is quadratic in the velocity, as in previous studies, and in particular the only difference with the result by Ref. [30] is the value of the coefficient  $k$ , which reads  $k = 6.26$  in their study. The origin of this discrepancy is explained in the SI. In the opposite limit of large Peclet, we find

$$\frac{F_{\text{lift}}}{F_0} \underset{\text{Pe} \gg 1}{\simeq} (\alpha_p + \alpha_w) \pi \left[ (52 - 45 \ln 3) \alpha_w + \frac{64 - 45 \ln 3}{2} \alpha_p \right] \quad (9)$$

This means that, for large Peclet, the force no-longer grows quadratically with the velocity but saturates to a finite value, that no longer depends on the velocity. The origin of this saturation can be traced back to Eq. (2),

where both the advective term  $\bar{\mathbf{U}}_{\parallel} \cdot \nabla N$  and the source term  $S_{\perp}$  are proportional to the imposed velocity. As a consequence, even if increasing the velocity increases the flux of ions escaping from the Debye layer due to the flow, it also increases the velocity in the advective component, and the resulting concentration gradients (and thus, the lift force) become independent of the imposed velocity when this one is large. To the best of our knowledge, this saturation of the force at high Peclet has not been identified before.

To compare with the experiments, we take into account the fact that the velocity is not constant but reads  $V(t) = V_0 \cos(\omega t)$ . The prediction of the theory for the time-averaged force in this case is:

$$F_{\text{lift}} = F_0 \Phi^*(\text{Pe}_*), \quad \Phi^*(u) = \frac{1}{2\pi} \int_0^{2\pi} d\tau \Phi(u \cos \tau), \quad (10)$$

where  $\text{Pe}_* = V_0 \sqrt{Rd} / D_e$ .

Figure 3a presents the results for the pure electroviscous lift force, obtained by subtracting the static double-layer force from the total force measured during lateral motion. The dashed line corresponds to the theoretical calculation based on our model [Eq. (6)]. The experimental data show good agreement with the theoretical predictions for distances larger than the Debye screening length. At shorter distances, a saturation of the force is observed, which is not captured by our model, as it is only valid in the regime of large separations. Figure 3b shows the measurements of the lift force obtained at two different velocities. It is clearly seen that the force increases with increasing velocity. Figure 3c depicts the results obtained at the same velocity but using two spheres of different radii, it shows that the larger the sphere, the greater the resulting force.

To rationalize our measurements, the experimentally measured electroviscous lift force was normalized by  $F_0$  and plotted as a master curve as a function of the Peclet

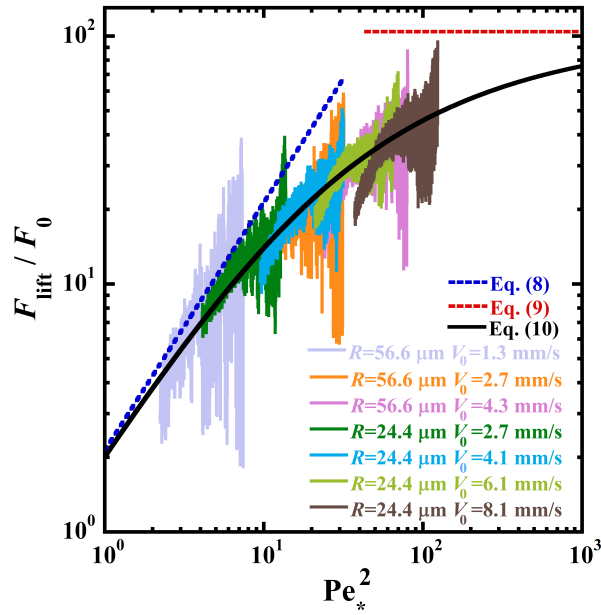


FIG. 4. Dimensionless lift force  $F_{\text{lift}}/F_0$  as a function of  $\text{Pe}_*^2 = V_0^2 R d / D_e^2$ . Experimental data obtained under various conditions are represented by different colors, for a range of  $d$  between 60 and 200 nm. The black line denotes the theoretical electroviscous lift force calculated from Eq. (10). Dash-dotted blue and red lines represent respectively the predictions at low and large Peclet numbers.

number, in accordance with the theoretical prediction Eq. (7). Figure 4 shows the measurements obtained for various velocities and sphere radii. We excluded distances  $d < 2\lambda \simeq 60$  nm (where the theory is not valid) and distances larger than 200 nm (where the noise is too high). The results follow the theoretical prediction of our model: as the Peclet number increases, the normalized force rises and tends to a saturation. In our experiments, however, we could not reach the saturation limit, because very large Peclet numbers correspond to large separations, where the measured force becomes extremely small and the signal-to-noise ratio consequently decreases. Nevertheless, our data unambiguously show a deviation of the rescaled force from a quadratic behavior with Peclet number. Note that, our model is derived in the framework of quasistatic velocities, which is justified in the SI where we check that the used values of  $\omega$  are sufficiently low to reach this regime.

In conclusion, we have presented measurements of the electroviscous lift force acting on an electrically charged sphere sliding along a charged solid surface in an aqueous solution. The lift force was investigated as a function of the separation distance between the sphere and the substrate, for various sliding velocities and two distinct sphere radii. Experimental results were compared with existing theoretical models for the electroviscous force; however, none of these models were able to accurately describe our observations. To address this discrepancy,

we derived a new analytical expression for the lift force based on Cox's formalism within the lubrication approximation framework, which predicts a new regime where the electroviscous force saturates for large driving velocity. Our experimental data show excellent quantitative agreement with this new theoretical prediction, in the absence of any fitting parameter. Altogether, our results provide the first robust and quantitative measurements of the electroviscous lift force that emerge between charged particles as a result of the motion of ions in viscous electrolytes in non-equilibrium conditions.

*Acknowledgments* - The authors thank Alois Würger for fruitful discussions. H. Zhang and Z. Zhang acknowledge the financial support of the China Scholarship Council during their stay in Bordeaux, which enabled them to carry out the experiments. The authors thank the French National Research Agency for the supporting grants MS-DOS (Grant No. ANR-25-CE06-3953-02) and EDDL (Grant No. ANR-19-CE30-0012).

*Author contributions* - A.M. conceived the project. T.G. developed the theory. H.Z., Z.Z. and A.M. performed the experiment and analysed the data. H.Z., A.M. and T.G. drafted the manuscript. All authors contributed to the interpretation of the results and the final version of the manuscript.

## SUPPLEMENTARY INFORMATION

Here, we provide the following elements:

- we write the general equations to be solved, their simplification in Cox's theory, and review existing results for the lift force (Section I),
- we show how to simplify these equations in the lubrication regime (Section II),
- we give explicit solutions of the equations in the regimes of small and large Peclet numbers, with a comparison with previous results when they exist (Section III for 2D and Section IV for 3D),
- we generalize the theory to take into account non-stationary effects, and we check that such effects are negligible for the parameters used in the experiments (Section V).

## I. PROBLEM STATEMENT

### A. Physical situation

We consider a charged sphere (if the spatial dimension is  $d_s = 3$ ) or a cylinder (if  $d_s = 2$ ) of radius  $R$ , close to a flat wall. Note that the particle will be called the

sphere (even in 2D). In principle, the sphere moves at a constant velocity near the wall, but, equivalently, we can consider that the sphere is fixed and the wall is moving at a constant velocity  $V$  in the  $x$  direction. The vertical  $z$  direction is perpendicular to the flat lower wall, and in 3D we call  $y$  the third spatial direction, so that  $(x, y, z)$  are Cartesian coordinates.

In the stationary state, the concentrations of cations ( $c_+$ ) and anions ( $c_-$ ), the hydrodynamic flow  $\mathbf{v}$ , and the electric potential  $\psi$  are governed by the following equations:

$$\nabla \cdot \mathbf{v} = 0, \quad -\nabla p + \eta \nabla^2 \mathbf{v} = q(c_+ - c_-) \nabla \psi, \quad (\text{S1})$$

$$\nabla^2 \psi = -q(c_+ - c_-)/\epsilon, \quad (\text{S2})$$

$$\mathbf{v} \cdot \nabla c_+ = D_+ \nabla \left( c_+ \frac{q \nabla \psi}{k_B T} + \nabla c_+ \right), \quad (\text{S3})$$

$$\mathbf{v} \cdot \nabla c_- = D_- \nabla \left( -c_- \frac{q \nabla \psi}{k_B T} + \nabla c_- \right), \quad (\text{S4})$$

Here,  $q > 0$  is the charge of a single cation, each anion carries the opposite charge  $-q$ .  $T$  is the temperature,  $k_B$  is Boltzmann's constant,  $\eta$  is the viscosity,  $\epsilon$  is the permittivity of the liquid,  $p$  the pressure, and  $D_\pm$  respectively represent the diffusivity of cations and anions.

At the lower wall, the flow velocity is the same as that of the wall,  $\mathbf{v} = V \hat{\mathbf{e}}_x$ , where  $\hat{\mathbf{e}}_i$  represents the unit vector in the direction  $i \in \{x, y, z\}$ . The velocity  $\mathbf{v}$  vanishes at the surface of the sphere. For the electric potential we consider constant potential conditions, with  $\psi = \psi_w$  at the lower wall (w) and  $\psi = \psi_p$  at the surface of the particle (p). Last, we have no flux conditions for ions at the solid surfaces

$$\mathbf{n} \cdot \left( (\pm c_\pm) \frac{q \nabla \psi}{k_B T} + \nabla c_\pm \right) = 0, \quad (\mathbf{r} \in \partial \Omega_s), \quad (\text{S5})$$

where  $\mathbf{n}$  is the normal vector to the solid surfaces, which point towards the liquid by convention. Note that  $\partial \Omega_s$ , with  $s \in \{w, p\}$ , denotes either the surface of the lower flat wall ( $s=w$ ) or the spherical particle's surface ( $s=p$ ). We also introduce  $d$  as the minimal distance between the sphere and the wall. Finally, far from the boundaries, the potential  $\psi$  vanishes, and the concentrations  $c_\pm$  tend to the value the concentration of ions  $c_\infty$  in the solution.

Our goal is to calculate the lift force on the sphere

$$F_{\text{lift}} = \int_{\partial \Omega_p} dS \mathbf{n} \cdot \boldsymbol{\Sigma} \cdot \hat{\mathbf{e}}_z, \quad (\text{S6})$$

where the stress tensor  $\boldsymbol{\Sigma}$  is the sum of the viscous stress and the Maxwell electromagnetic stress:

$$\boldsymbol{\Sigma} = -p \mathbf{I} + \eta [\nabla \mathbf{v} + (\nabla \mathbf{v})^\dagger] + \epsilon \left( \mathbf{E} \otimes \mathbf{E} - \frac{\mathbf{E}^2}{2} \mathbf{I} \right), \quad (\text{S7})$$

with  $\nabla \mathbf{v}$  the gradient of  $\mathbf{v}$ ,  $\mathbf{I}$  the identity tensor and  $\mathbf{E} = -\nabla \psi$  the electric field. We also introduce the Debye screening length as

$$\lambda = \sqrt{\frac{k_B T \epsilon}{2q^2 c_\infty}}. \quad (\text{S8})$$

## B. Existing results for the sphere wall geometry

We report existing results for the lift force for the sphere-wall geometry. We first consider the theory of Prieve and co-workers, who calculated the Maxwell stress (MS) on the spherical particle in the regime  $\lambda \ll d \ll R$ , giving rise to the force [16]

$$F_{\text{MS}} = \frac{\epsilon^3 \pi V^2 R}{K^2 d^3} \left[ 0.384 \left( \frac{\psi_p + \psi_w}{2} \right)^2 + 0.181 \frac{(\psi_p - \psi_w)(\psi_p + \psi_w)}{2} + 0.024 (\psi_p - \psi_w)^2 \right] \quad (\text{S9})$$

where  $K = \epsilon(D_+ + D_-)/(2\lambda^2)$  [16] is the conductivity of the liquid. As can be seen in Fig. 2b of the main text, this force cannot explain the increase of lift force due to the lateral oscillation of the sphere. This may not be surprising since it was already pointed out [25] that the electric field induced by the hydrodynamic flow generates an additional flow, associated to a viscous stress tensor that dominates over the Maxwell electric stress. In this reference, a general formalism was introduced to calculate this viscous stress in the limit of a small Debye screening length. Using this formalism in the cylinder-wall geometry, under the lubrication approximation, for small enough velocities and assuming large distances ( $d \gg \lambda$ ), the expression of the force due to the electro-viscous stress was calculated. By further applying the Derjaguin approximation, Warszynski *et al.* [28, 29] obtained the electroviscous lift force acting on the sphere from cylinder-wall geometry as

$$F_{\text{VS}} = \frac{\epsilon \pi \lambda^2}{D_e^2} \left( \frac{k_B T}{q} \right)^2 \frac{V^2 R^2}{d^2} (D_+ I_w^- + D_- I_w^+) \times \frac{(9D_+ I_p^- + D_+ I_w^- + 9D_- I_p^+ + D_- I_w^+)}{6(D_+ + D_-)^2} + \frac{\epsilon \pi \lambda^4}{D_e^2} \left( \frac{k_B T}{q} \right)^2 \frac{V^2 R}{d^3} \times \frac{7(D_+ I_p^- - D_- I_p^+)^2 + (D_+ I_w^- - D_- I_w^+)^2}{30(D_+ + D_-)^2} + \frac{4D_+ D_- \left( \frac{D_+}{D_-} I_p^- I_w^+ + \frac{D_-}{D_+} I_p^+ I_w^- - I_p^+ I_w^- - I_p^- I_w^+ \right)}{30(D_+ + D_-)^2} \quad (\text{S10})$$

where  $I_s^\pm = \mp \Psi_s + 4 \ln \cosh \left( \frac{\Psi_s}{4} \right)$ ,  $\Psi_s = \psi_s q / k_B T$ , and  $D_e = \frac{2D_+ D_-}{D_+ + D_-}$  denotes the effective diffusion coefficient. The first term of Eq. (S10) arises from viscous stress and the second term is due to the Maxwell stress. Within the range of distances for which this expression is valid ( $\lambda \ll d$ ), the second term is much smaller than the first one, with their ratio scaling as  $\lambda^2/Rd$ . As observed in Fig. 2b in the main text, this force is about one order of magnitude larger than the experimentally observed lift force.

Finally, Tabatabaei *et al.* used the Lorentz reciprocal theorem to calculate the electroviscous lift force acting on a cylinder [31] and a sphere [30] sliding along a planar wall at small velocity in the lubrication regime. In the sphere-wall geometry, they obtained

$$F_{\text{VS}} = \frac{24\pi\epsilon}{5} \left( \frac{k_B T \lambda V R}{qd} \right)^2 \times \left\{ \frac{1}{5} \left( \frac{G_p}{D_+} + \frac{H_p}{D_-} + \frac{G_w}{D_+} + \frac{H_w}{D_-} \right)^2 + 1.667 \left[ \left( \frac{G_p}{D_+} + \frac{H_p}{D_-} \right)^2 - \left( \frac{G_w}{D_+} + \frac{H_w}{D_-} \right)^2 \right] \right\}, \quad (\text{S11})$$

see Eq (6.27) in Ref. [30]. Here the dimensionless parameters  $(G_p, H_p)$  on the sphere and  $(G_w, H_w)$  on the substrates are defined as

$$G_s = \ln \frac{1 + e^{-\Psi_s/2}}{2}, \quad H_s = \ln \frac{1 + e^{\Psi_s/2}}{2}. \quad (\text{S12})$$

For the parameters corresponding to our experiments, the lift force (S11) is negative, which disagrees with our observations. We show in Section IV B 2 that, although the above formula is exact for small velocities when the zeta potentials of the particle and the wall are identical, it is not valid for distinct zeta potentials due to a subtle mathematical issue of uniform convergence.

### C. The limit of small Debye length: Cox's Equations

In the limit  $\lambda \rightarrow 0$ , meaning that  $\lambda$  is smaller than all other length scales of the system, the potential  $\psi$  is large only at distances less than  $\lambda$  from the charged walls. Far from the boundaries, the equations for the ionic concentrations and the potentials are considerably simplified, and the physical mechanisms at play in the electrostatic layer are taken into account via effective boundary conditions. A complete theory, including the flow induced by the motion of ions, was developed by Cox in Ref. [25]. Since we will use this formalism as a starting point for our study, we recall it here.

First, due to the linearity of Stokes equation, we can separate the flow field into two contributions:

$$\mathbf{v} = \mathbf{u} + \mathbf{u}^* \quad (\text{S13})$$

where  $\mathbf{u}$  is the flow induced by the motion of the lower wall only, *i.e.* in the absence of ions, and  $\mathbf{u}^*$  is the flow induced by the motion of ions, which satisfies Eq. (S1) but vanishes at the boundaries.

Next, in the limit  $\lambda \rightarrow 0$ , electroneutrality is achieved everywhere ( $c_+ = c_- = c$ ) except in the vicinity of the charged walls [25]. At distances larger than  $\lambda$  from the boundaries, the concentrations of cations and anions and

the electric potential satisfy the bulk equations:

$$\mathbf{u} \cdot \nabla c = D_e \nabla^2 c, \quad (\text{S14})$$

$$\nabla^2 \left( \frac{\psi q}{k_B T} + \beta \frac{c}{c_\infty} \right) = 0, \quad (\text{S15})$$

these are equations (9.6), (9.7), (9.8) in Ref. [25]. This equation takes into account the fact that the flow  $\mathbf{u}^*$  induced by the dynamics of ions is much lower than the imposed flow  $\mathbf{u}$ . Here,  $\beta$  is the relative difference of diffusivities between cations and anions, and  $D_e$  is the effective ionic diffusivity:

$$\beta = \frac{D_+ - D_-}{D_+ + D_-}, \quad D_e = \frac{2D_+ D_-}{D_+ + D_-}. \quad (\text{S16})$$

The effective boundary conditions at the surfaces  $\partial\Omega_s$ ,  $s \in \{w, p\}$ , are

$$\partial_n c = -\frac{2c_\infty \lambda^2 s_\perp^s}{D_e} \alpha_s, \quad (\text{S17})$$

$$\partial_n \psi = \frac{2\lambda^2 s_\perp^s k_B T}{qD_e} [\Psi_s + 4\beta \ln \cosh(\Psi_s/4)], \quad (\text{S18})$$

see equations (8.7), (8.9), (9.6) and (9.8) in Ref. [25]. Here, we recall that  $\Psi_s = \psi_s q/k_B T$  is the dimensionless potential at the surface  $\partial\Omega_s$ . The dimensionless parameter  $\alpha_s$  depends only on the zeta potential of the surface and the difference of ionic diffusivities:

$$\alpha_s = \beta \Psi_s + 4 \ln \cosh(\Psi_s/4), \quad (\text{S19})$$

and  $s_\perp$  is defined near each solid boundary as

$$s_\perp = \partial_n^2(\mathbf{u} \cdot \mathbf{n})/2, \quad (\text{S20})$$

where  $\partial_n = \mathbf{n} \cdot \nabla$ . Last, since electroneutrality holds in the bulk, the flow  $\mathbf{u}^*$  induced by the motion of the ions satisfy the usual Stokes equations,

$$\nabla \cdot \mathbf{u}^* = 0, \quad -\nabla p^* + \eta \nabla^2 \mathbf{u}^* = 0. \quad (\text{S21})$$

However, in the electrostatic Debye layer electroneutrality is broken, this induces an effective slip velocity  $\mathbf{u}^* = \mathbf{u}_s^*$  at the boundaries, with

$$\mathbf{u}_s^* = \frac{2c_\infty k_B T \lambda^2}{\eta} \left\{ -4 \ln \cosh \frac{\Psi_s}{4} \nabla_s \frac{c}{c_\infty} + \Psi_s \nabla_s \frac{\psi q}{k_B T} \right\}, \quad (\mathbf{r} \in \partial\Omega_s), \quad (\text{S22})$$

see Eqs. (2.10) and (10.7) in Ref. [25]. Here,

$$\nabla_s = \nabla - \mathbf{n} \partial_n. \quad (\text{S23})$$

These equations are obtained by using a matched asymptotics expansion analysis in the limit of small  $\lambda$  when the Peclet number  $\ell V/D_e$  is taken constant, with  $\ell$  a characteristic length scale of the problem ( $R, d, \dots$ ). Of note, the validity of these equations has been questioned in

Ref. [26] where it was noted that Cox implicitly assumed that the Hartmann number was constant in the limit of small Debye length, which is not physical. This assumption is mainly used to justify the fact that the perpendicular flow generated by the ions  $u_{\perp}^*$  in the Debye layer is negligible compared to the imposed flow perpendicular to the interface. This approximation can be justified self-consistently. The imposed perpendicular flow at distances  $\lambda$  from the walls reads  $u_{\perp} \sim V(\lambda/\ell)^2$ . On the other hand, using the incompressibility condition one can estimate  $u_{\perp}^* \sim u_{\parallel}^*(\lambda/\ell)$ , so that  $u_{\perp}^* \sim k_B T c_{\infty} \lambda^5 / (\eta \ell^4)$ , see Eq. (S22). Comparing the two leads to

$$\frac{u_{\perp}^*}{u_{\perp}} \sim \frac{k_B T c_{\infty} \lambda^2}{\eta D_e} \times \frac{D_e}{\ell V} \times \frac{\lambda}{\ell} \quad (\text{S24})$$

Now, the term  $D_e/(\ell V) = \text{Pe}^{-1}$  is of the order one in the theory,  $c_{\infty} \lambda^2$  can be identified as of the order of the inverse of the Bjerrum length, and  $k_B T/(\eta D_e)$  is of the order of the ionic radius. As a consequence, as noted in Ref. [26]  $k_B T c_{\infty} \lambda^2 / (\eta D_e) \simeq \mathcal{O}(1)$ , irrespective of the ionic concentration or the viscosity. Hence,  $u_{\perp}^*/u_{\perp} \sim \lambda/\ell \ll 1$  and we conclude that Cox equations are justified in the limit of small  $\lambda$  at constant Peclet. This remark is consistent with the fact that Cox equations were actually recovered in the case  $D_+ = D_-$  when the Peclet number is moderate in Ref. [27].

## II. COX'S EQUATIONS IN THE LUBRICATION REGIME $d \ll R$

Here, we present an analysis of Cox's equations, presented in Section IC, in the lubrication regime  $d \ll R$ , with the condition  $\lambda \ll d$ . We define  $l = \sqrt{Rd}$  the characteristic length in the lateral direction, and we use rescaled coordinates

$$X = x/l, \quad Y = y/l, \quad Z = z/d, \quad (\text{S25})$$

so that the equation for the surface is

$$Z = H(X, Y) = \begin{cases} 1 + \frac{1}{2}(X^2 + Y^2) & (\text{if } d_s = 3) \\ 1 + \frac{1}{2}X^2 & (\text{if } d_s = 2) \end{cases} \quad (\text{S26})$$

where the dimensionless local distance  $H$  between the sphere and the surface is defined by the above equation. We introduce the small parameter  $\varepsilon$  as

$$\varepsilon = d/R \ll 1. \quad (\text{S27})$$

Note that we develop the formalism in three-dimensions ( $d_s = 3$ ), the two dimensional case ( $d_s = 2$ ) will be obviously deduced by omitting the coordinate  $Y$ .

### A. Lubrication approximation for the flow induced by the motion of the wall

Here we describe the flow  $(u_x, u_y, u_z)$ , associated with the pressure field  $p$ , generated by the motion of the wall

at velocity  $V$ , in the absence of ions. This is a standard hydrodynamic problem [39, 40]. In lubrication theory we have the scaling

$$u_x = V U_X(X, Y, Z), \quad u_y = V U_Y(X, Y, Z), \quad (\text{S28})$$

$$u_z = V \varepsilon^{1/2} U_Z(X, Y, Z), \quad p = \frac{\eta V l}{d^2} P(X, Y, Z). \quad (\text{S29})$$

Inserting this ansatz into Stokes equations, we obtain

$$-\nabla_{\parallel} P + \partial_Z^2 \mathbf{U}_{\parallel} = 0, \quad -\partial_Z P = 0, \quad (\text{S30})$$

$$\nabla_{\parallel} \cdot \mathbf{U}_{\parallel} + \partial_Z U_Z = 0, \quad (\text{S31})$$

where  $\mathbf{U}_{\parallel} = U_X \hat{\mathbf{e}}_x + U_Y \hat{\mathbf{e}}_y$  and  $\nabla_{\parallel} = \partial_X \hat{\mathbf{e}}_x + \partial_Y \hat{\mathbf{e}}_x$ . Note that  $\nabla_{\parallel}$  should not be confounded with  $\nabla_s$  defined in Eq. (S23). Noting that  $P$  does not depend on  $Z$ , the solution to Eq. (S30) reads

$$\mathbf{U}_{\parallel} = \frac{H - Z}{H} \hat{\mathbf{e}}_x + (\nabla_{\parallel} P) \frac{Z(H - Z)}{2}. \quad (\text{S32})$$

Inserting this expression into the continuity equation (S31), using  $U_Z(0) = 0$  and integrating over  $Z$  leads to

$$U_Z = -\frac{Z^2 \partial_X H}{2H^2} + \nabla_{\parallel} \cdot \left[ (\nabla_{\parallel} P) \left( -\frac{Z^3}{6} + \frac{Z^2 H}{4} \right) \right]. \quad (\text{S33})$$

The condition  $U_Z(H) = 0$  at the second boundary leads to an equation for the pressure

$$\frac{\partial_X H}{2} = \nabla_{\parallel} \cdot \left[ (\nabla_{\parallel} P) \frac{H^3}{12} \right]. \quad (\text{S34})$$

In the case of a sphere (in 3D) or a cylinder (in 2D), the only physically acceptable solution is [39, 40]

$$P = \begin{cases} -6X/(5H^2) & (d_s = 3), \\ -2X/H^2 & (d_s = 2). \end{cases} \quad (\text{S35})$$

Now, the quantities  $s_{\perp}$ , defined in Eq. (S20), can be identified. The normal pointing towards the liquid at the sphere's surface is

$$\mathbf{n} \simeq -\hat{\mathbf{e}}_z + \sqrt{\varepsilon} \nabla_{\parallel} H, \quad (\text{S36})$$

so that

$$\mathbf{n} \cdot \mathbf{u} = V \sqrt{\varepsilon} (-U_Z + \nabla_{\parallel} H \cdot \mathbf{U}_{\parallel}). \quad (\text{S37})$$

We thus find that  $s_{\perp}$  scales as

$$s_{\perp} = \frac{V \sqrt{\varepsilon}}{d^2} S_{\perp}(X, Y), \quad (\text{S38})$$

where  $S_{\perp}$  can be identify in terms of the rescaled flow at the sphere's surface:

$$S_{\perp}^p(X, Y) = \lim_{Z \rightarrow H} \frac{-U_Z + \nabla_{\parallel} H \cdot \mathbf{U}_{\parallel}}{(H - Z)^2}. \quad (\text{S39})$$

For the wall, we follow the same reasoning with  $\mathbf{n} = \hat{\mathbf{e}}_z$ , leading to

$$S_{\perp}^s(X, Y) = \lim_{Z \rightarrow 0} U_Z/Z^2. \quad (\text{S40})$$

In the three-dimensional case, the values  $S_{\perp}^s$  are

$$S_{\perp}^w = -\frac{2X(X^2 + Y^2 - 4)}{5H^3}, \quad (\text{S41})$$

$$S_{\perp}^p = \frac{X(X^2 + Y^2 + 26)}{10H^3}. \quad (\text{S42})$$

In the two-dimensional case, we obtain

$$S_{\perp}^w = -\frac{8X(X^2 - 2)}{(X^2 + 2)^3}, \quad S_{\perp}^p = -\frac{4X(X^2 - 6)}{(X^2 + 2)^3}. \quad (\text{S43})$$

### B. Lubrication approximation for the ionic concentration $c$

Let us introduce the Peclet number associated to the length scale  $l$ , defined as

$$\text{Pe} = \frac{V\sqrt{dR}}{D_e}, \quad (\text{S44})$$

so that the advection diffusion (S14) for  $c$  becomes

$$\text{Pe} \varepsilon(U_X \partial_X c + U_Y \partial_Y c + U_Z \partial_Z c) = \partial_Z^2 c + \varepsilon \nabla_{\parallel}^2 c. \quad (\text{S45})$$

Here we keep the parameter  $\text{Pe}$  constant when taking the limit  $d/R \rightarrow 0$ . For the boundary conditions at the sphere's surface, we note that, for any field  $\phi$ ,

$$\mathbf{n} \cdot \nabla \phi = \frac{1}{d}[-\partial_Z \phi + \varepsilon(\nabla_{\parallel} H) \cdot (\nabla_{\parallel} \phi)]. \quad (\text{S46})$$

Using the above expression and Eq. (S38), the boundary condition (S17) becomes

$$[-\partial_Z c + \varepsilon(\nabla_{\parallel} H) \cdot \nabla_{\parallel} c]_{Z=H} = -\frac{2c_{\infty}\lambda^2 V}{\sqrt{dR}D_e} S_{\perp}^p \alpha_p, \quad (\text{S47})$$

$$(\partial_Z c)_{Z=0} = -2\frac{c_{\infty}\lambda^2 V}{d^{1/2}\sqrt{R}D_e} S_{\perp}^w \alpha_w. \quad (\text{S48})$$

Equations (S45), (S47), (S48) suggest looking for solutions under the form

$$c = c_{\infty} + \frac{c_{\infty}\lambda^2}{d^2}(N + \varepsilon N_1 + \dots), \quad (\text{S49})$$

so that, at leading order in  $\varepsilon$ ,

$$\partial_Z^2 N = 0, \quad (\partial_Z N)_{Z=0} = (\partial_Z N)_{Z=H} = 0, \quad (\text{S50})$$

which means that  $N$  depends only on  $X, Y$ . At next order we have

$$\text{Pe} \mathbf{U}_{\parallel} \cdot \nabla_{\parallel} N = \partial_Z^2 N_1 + \nabla_{\parallel}^2 N, \quad (\text{S51})$$

$$(-\partial_Z N_1 + \nabla_{\parallel} H \cdot \nabla_{\parallel} N)_{Z=H} = -2\alpha_p \text{Pe} S_{\perp}^p, \quad (\text{S52})$$

$$(\partial_Z N_1)_{Z=0} = -2\alpha_w \text{Pe} S_{\perp}^w. \quad (\text{S53})$$

Integrating Eq. (S51) over  $Z \in [0, H]$  and using the boundary conditions Eqs. (S52) and (S53), we obtain

$$\text{Pe} \bar{\mathbf{U}}_{\parallel} \cdot \nabla_{\parallel} N = \nabla_{\parallel} \cdot (H \nabla_{\parallel} N) + 2\text{Pe}(\alpha_w S_{\perp}^w + \alpha_p S_{\perp}^p). \quad (\text{S54})$$

where  $\bar{\mathbf{U}}_{\parallel} = \int_0^H dZ \mathbf{U}_{\parallel}$ .  $N$  satisfies an effective stationary advection-diffusion equation, with an effective velocity field  $\bar{\mathbf{U}}_{\parallel}$  that is incompressible due to Eq. (S34), and an external source term. The effective flow  $\bar{\mathbf{U}}_{\parallel}$  can be calculated from Eq. (S32), so that

$$\bar{\mathbf{U}}_{\parallel} = \frac{H}{2} \hat{\mathbf{e}}_x - \frac{H^3}{12} \nabla_{\parallel} P. \quad (\text{S55})$$

In the three-dimensional case, using (S35), we obtain

$$\bar{U}_X = \frac{3}{5} + \frac{X^2 + 3Y^2}{10}, \quad \bar{U}_Y = -\frac{XY}{5}, \quad (\text{S56})$$

whereas in the two-dimensional case, we obtain

$$\bar{U}_X = 2/3. \quad (\text{S57})$$

### C. Lubrication approximation for the electric potential

Next, we seek an effective equation for the electric potential. Eq. (S15) suggests that it is simpler to work with the reduced potential  $\mathcal{A}$  defined as

$$\mathcal{A} = \psi + \beta \frac{k_B T}{qc_{\infty}} c, \quad (\text{S58})$$

which satisfies  $\nabla^2 \mathcal{A} = 0$ . The boundary conditions for  $\mathcal{A}$  are obtained by combining Eqs. (S17) and (S18) :

$$\partial_n \mathcal{A} = 2 \frac{\lambda^2 k_B T S_{\perp}^s}{D_e q} (1 - \beta^2) \Psi_s. \quad (\text{S59})$$

Using Eqs. (S46) and (S38), we can write

$$(-\partial_Z \mathcal{A} + \varepsilon \nabla_{\parallel} H \cdot \nabla_{\parallel} \mathcal{A})_H = \frac{2k_B T \lambda^2 \text{Pe} S_{\perp}^p (1 - \beta^2) \Psi_p}{qd^2} \varepsilon \quad (\text{S60})$$

$$(\partial_Z \mathcal{A})_{Z=0} = \frac{2k_B T \lambda^2 \text{Pe} S_{\perp}^w (1 - \beta^2) \Psi_w}{qd^2} \varepsilon. \quad (\text{S61})$$

We look for solutions scaling as

$$\mathcal{A} = \frac{k_B T \lambda^2}{qd^2} (A + \varepsilon A_1 + \dots) \quad (\text{S62})$$

The equations for  $A$  and  $A_1$  are exactly the same as those for  $N$  and  $N_1$  in the absence of advective term, if one replaces the factors  $-\alpha_s$  by  $(1 - \beta^2)\Psi_s$ . We thus directly write

$$\nabla_{\parallel} \cdot (H \nabla_{\parallel} A) = 2(1 - \beta^2) \text{Pe} (\Psi_p S_{\perp}^p + \Psi_w S_{\perp}^w). \quad (\text{S63})$$

#### D. Lubrication approximation for the flow induced by the motion of ions

We now extend the lubrication approximation to the flow  $\mathbf{u}^*$  induced by the motion of ions. First, we note that surface nabla operator  $\nabla_s$ , given by Eq. (S23), when applied to  $c$  given by Eq. (S49) at the sphere's surface, reads

$$\nabla_s c = \frac{c_\infty \lambda^2}{d^2 l} [\nabla_{\parallel} N + (\nabla_{\parallel} N \cdot \nabla_{\parallel} H) \sqrt{\varepsilon} \hat{\mathbf{e}}_z + \mathcal{O}(\varepsilon)], \quad (\text{S64})$$

where we have used the fact that  $N$  depends only on  $X, Y$ . This expression is valid at the surface of the particle, while at the wall the same expression holds without the term  $\nabla_{\parallel} H$ . Note that, in the above expression, the vertical component comes from the fact that the tangent to the surface is not exactly in the horizontal plane. Using this result and a similar expression for the potential, we see that the slip velocity in Eq. (S22), at the sphere's surface, reads

$$\mathbf{u}_p^* = v^* \left\{ -\alpha_p \nabla_{\parallel} N + \Psi_p \nabla_{\parallel} A + \sqrt{\varepsilon} (\nabla_{\parallel} H) \cdot (-\alpha_p \nabla_{\parallel} N + \Psi_p \nabla_{\parallel} A) \hat{\mathbf{e}}_z \right\}, \quad (\text{S65})$$

with the characteristic induced velocity

$$v^* = \frac{2c_\infty k_B T \lambda^4}{\eta d^2 l} = \frac{\epsilon (k_B T)^2 \lambda^2}{\eta q^2 d^2 l}. \quad (\text{S66})$$

Similarly, at the wall, the slip velocity is

$$\mathbf{u}_w^* = v^* \left\{ -\alpha_w \nabla_{\parallel} N + \Psi_w \nabla_{\parallel} A \right\}, \quad (\text{S67})$$

Choosing  $v^*$  as the velocity scale for the flow induced by the ions, we have the following structure for this flow in the lubrication regime:

$$u_x^* = v^* U_X^*, \quad u_y^* = v^* U_Y^* \quad (\text{S68})$$

$$u_z^* = v^* \sqrt{\varepsilon} U_Z^*, \quad p^* = \frac{\eta v^* l}{d^2} P^*. \quad (\text{S69})$$

The equations for the rescaled induced flow are

$$-\nabla_{\parallel} P^* + \partial_Z^2 \mathbf{U}_{\parallel}^* = 0, \quad \partial_Z P^* = 0, \quad (\text{S70})$$

$$\nabla_{\parallel} \cdot \mathbf{U}_{\parallel}^* + \partial_Z U_Z^* = 0, \quad (\text{S71})$$

The associated boundary conditions are obtained from Eqs. (S65) and (S67) and read

$$(\mathbf{U}_{\parallel}^*)_{Z=0} = -\alpha_w \nabla_{\parallel} N + \Psi_w \nabla_{\parallel} A, \quad (\text{S72})$$

$$(\mathbf{U}_{\parallel}^*)_{Z=H} = -\alpha_p \nabla_{\parallel} N + \Psi_p \nabla_{\parallel} A, \quad (\text{S73})$$

$$(U_Z^*)_{Z=0} = 0, \quad (\text{S74})$$

$$(U_Z^*)_{Z=H} = \nabla_{\parallel} H \cdot (-\alpha_p \nabla_{\parallel} N + \Psi_p \nabla_{\parallel} A). \quad (\text{S75})$$

Noting that  $P^*$  does not depend on  $Z$ , integrating Eq. (S70) over  $Z$  and using the above boundary conditions leads to

$$\mathbf{U}_{\parallel}^* = \frac{(\nabla_{\parallel} P^*) Z (Z - H)}{2} - (\alpha_w \nabla_{\parallel} N - \Psi_w \nabla_{\parallel} A) \frac{H - Z}{H} - (\alpha_p \nabla_{\parallel} N - \Psi_p \nabla_{\parallel} A) \frac{Z}{H}. \quad (\text{S76})$$

We insert this expression into the continuity equation Eq. (S71) and integrate the resulting equation over  $Z \in [0, H]$ ; with the use of Eq. (S75) this leads to

$$\frac{\nabla_{\parallel} (H^3 \nabla_{\parallel} P^*)}{12} = -\frac{1}{2} (\alpha_w + \alpha_s) \nabla_{\parallel} \cdot (H \nabla_{\parallel} N) + \frac{\Psi_w + \Psi_p}{2} \nabla_{\parallel} \cdot (H \nabla_{\parallel} A). \quad (\text{S77})$$

This equation, with the condition  $P^* \rightarrow 0$  at infinity, defines the pressure  $P^*$  associated to the induced flow.

#### E. Expression of the electroviscous lift force

The lift force can be evaluated at  $Z = 0$  (above the electrostatic Debye layer). We find that at leading order, the lift force comes from the pressure associated to the flow  $\mathbf{u}^*$  induced by the motion of ions:

$$F_{\text{lift}} = \int d\mathbf{r} p^* = \frac{\eta v^* l^{d_s}}{d^2} \int d\mathbf{R}_{\parallel} P^*, \quad (\text{S78})$$

where  $d\mathbf{R}_{\parallel} = dX dY$  if  $d_s = 3$  and  $d\mathbf{R}_{\parallel} = dX$  if  $d_s = 2$ . Note that, if  $d_s = 2$ , the calculated force is in fact the force per unit length. We define a dimensionless force

$$\Phi(\text{Pe}) = \int d\mathbf{R}_{\parallel} P^*(\mathbf{R}_{\parallel}). \quad (\text{S79})$$

With this definition, the lift force reads

$$F_{\text{lift}} = \epsilon \left( \frac{k_B T \lambda}{q d^2} \right)^2 l^{d_s-1} \Phi(\text{Pe}). \quad (\text{S80})$$

We also define the Maxwell (M) component of the force, whose leading order component reads [see Eqs. (S58), (S62) and (S7)]:

$$F_{\text{lift}}^M = \epsilon \left( \frac{k_B T \lambda^2}{q d^2} \right)^2 \frac{l^{d_s}}{2l^3} \int d\mathbf{R}_{\parallel} [\nabla_{\parallel} (A - \beta N)]^2. \quad (\text{S81})$$

It is instructive to compare the magnitude of this Maxwell contribution to the main contribution (S80)

$$\frac{F_{\text{lift}}^M}{F_{\text{lift}}} \sim \frac{\lambda^2}{Rd} \ll 1, \quad (\text{S82})$$

meaning that, when  $\lambda \ll \sqrt{Rd}$ , the viscous contribution to the lift force dominates over the contribution of Maxwell's stress.

Let us simplify the expression for the force. First, an integration by part in Eq. (S79) leads to

$$\Phi = -\frac{1}{d_s - 1} \int d\mathbf{R}_{\parallel} \mathbf{R}_{\parallel} \cdot \nabla_{\parallel} P^*(\mathbf{R}_{\parallel}), \quad (\text{S83})$$

where we have assumed that  $P^*$  decays fast enough for large  $|\mathbf{R}_{\parallel}|$  (as is the case in practice). Note that we have used  $\nabla_{\parallel} \cdot \mathbf{R}_{\parallel} = d_s - 1$ . For a parabolic surface, we have  $\mathbf{R}_{\parallel} = \nabla_{\parallel} H$ , so that we can write

$$\Phi = -\frac{1}{d_s - 1} \int d\mathbf{R}_{\parallel} \frac{\nabla_{\parallel} H}{H^3} \cdot (H^3 \nabla_{\parallel} P^*). \quad (\text{S84})$$

Applying again the divergence formula leads to

$$\Phi = -\frac{1}{2(d_s - 1)} \int d\mathbf{R}_{\parallel} \frac{\nabla_{\parallel} \cdot (H^3 \nabla_{\parallel} P^*)}{H^2}. \quad (\text{S85})$$

Using Eq. (S77) for the rescaled pressure, we obtain

$$\Phi = \frac{3}{d_s - 1} \int \frac{d\mathbf{R}_{\parallel}}{H^2} \left[ (\alpha_w + \alpha_p) \nabla_{\parallel} \cdot (H \nabla_{\parallel} N) - (\Psi_w + \Psi_s) \nabla_{\parallel} \cdot (H \nabla_{\parallel} A) \right]. \quad (\text{S86})$$

The term involving  $A$  can then be simplified by using Eq. (S63) and one can easily check that

$$\int d\mathbf{R}_{\parallel} \frac{S_{\perp}^w}{H^2} = \int d\mathbf{R}_{\parallel} \frac{S_{\perp}^p}{H^2} = 0, \quad (\text{S87})$$

so that the contribution of the term  $A$  to the force is exactly zero. Ignoring the contribution of the term  $A$  in Eq. (S86) and applying once again the divergence formula, we obtain

$$\Phi = \frac{6(\alpha_w + \alpha_p)}{d_s - 1} \int d\mathbf{R}_{\parallel} \frac{(\nabla_{\parallel} H) \cdot (\nabla_{\parallel} N)}{H^2}. \quad (\text{S88})$$

We may also write an alternative form of this rescaled force by using Eqs. (S86), (S54) and (S87):

$$\Phi = \frac{3Pe}{(d_s - 1)} \int \frac{d\mathbf{R}_{\parallel}}{H^2} \bar{\mathbf{U}}_{\parallel} \cdot \nabla_{\parallel} N. \quad (\text{S89})$$

In summary, in the regime  $\lambda \ll d \ll R$ , the lift force is given by Eqs. (S80) and (S88), where  $N$  is the solution of Eq. (S54).

### III. EXPLICIT SOLUTION IN 2D

In the two-dimensional case,  $d_s = 2$ , the lift force (per unit length in the lateral direction of the cylinder) reads

$$F_{\text{lift}} = \epsilon \left( \frac{k_B T \lambda}{q} \right)^2 \frac{\sqrt{R}}{d^{7/2}} \Phi(\text{Pe}). \quad (\text{S90})$$

To find  $\Phi$ , one needs to solve Eq. (S54), which is a first order ordinary differential equation for  $\partial_X N(X)$  and can

be solved with standard methods. After finding the solution with  $\int_{-\infty}^{\infty} dX N'(X) = 0$  (which is necessary to impose, so that  $N$  tends to the same on both sides of the cylinder), we obtain for the dimensionless force:

$$\Phi = \frac{9\pi(\alpha_p + \alpha_w)Pe^2 [2Pe^2(3\alpha_p + \alpha_w) + 9(9\alpha_p + \alpha_w)]}{4\sqrt{2} (Pe^2 + 18) (2Pe^2 + 9)}. \quad (\text{S91})$$

In particular, at small Peclet numbers, we find

$$\Phi(\text{Pe} \rightarrow 0) \simeq \frac{\pi(\alpha_p + \alpha_w)(9\alpha_p + \alpha_w)}{8\sqrt{2}} Pe^2. \quad (\text{S92})$$

At very high Peclet numbers, we obtain

$$\Phi(\text{Pe} \rightarrow \infty) \simeq \frac{9\pi(\alpha_p + \alpha_w)(3\alpha_p + \alpha_w)}{4\sqrt{2}}. \quad (\text{S93})$$

To compare with the results of Ref. [31] it is useful to introduce their notations:

$$\begin{aligned} G_s &= \ln \frac{1 + e^{-\Psi_s/2}}{2} = -\frac{\Psi_s}{4} + \ln \cosh(\Psi_s/4) \\ &= \frac{\alpha_s}{4} - \frac{\Psi_s(1 + \beta)}{4}, \end{aligned} \quad (\text{S94})$$

$$\begin{aligned} H_s &= \ln \frac{1 + e^{\Psi_s/2}}{2} = \frac{\Psi_s}{4} + \ln \cosh(\Psi_s/4) \\ &= \frac{\alpha_s}{4} + \frac{\Psi_s(1 - \beta)}{4}, \end{aligned} \quad (\text{S95})$$

with  $s \in \{w, p\}$ . Using this, we can show that

$$\frac{G_s}{D_+} + \frac{H_s}{D_-} = \frac{\alpha_s}{2D_e}. \quad (\text{S96})$$

Using this identity, we notice that the result of Ref. [31], obtained for small velocities, is the same as Eq. (S92). Our result Eq. (S91) however is more general since it covers the case of finite Peclet numbers. In another paper [29], a similar result was obtained but with differences in the prefactor, with a very similar approach based on Cox's equations. The difference comes from the presence of a subtle mistake in Ref. [29]: between their equations (51) and (52), it is claimed that the vertical component of the induced flow  $\mathbf{u}^*$  vanishes at the solid walls, whereas this is not true for the condition at the cylinder, see Eq. (S75). This mistake was not present in Ref. [31] since their analysis avoided the direct calculation of the flow was not calculated explicitly by using a reciprocal theorem to calculate the lift force.

### IV. EXPLICIT SOLUTION IN 3D

#### A. Structure of the solution

In 3D, the lift force reads

$$F_{\text{lift}} = \epsilon \left( \frac{k_B T \lambda}{q} \right)^2 \frac{R}{d^3} \Phi. \quad (\text{S97})$$

Looking at Eqs. (S88) and (S54), it is clear that the dimensionless force can be put under the form

$$\Phi = (\alpha_p + \alpha_w)(\Phi_w \alpha_w + \Phi_p \alpha_p), \quad (\text{S98})$$

where

$$\Phi_s = 3 \int d\mathbf{R}_\parallel \frac{\nabla_\parallel H \cdot \nabla_\parallel N_s}{H^2}, \quad s \in \{p, w\}, \quad (\text{S99})$$

and  $N_s$  is the solution of Eq. (S54) when only the source term corresponding to the surface  $s$  is present, *i.e.*  $N_s$  satisfies

$$\text{Pe} \bar{\mathbf{U}}_\parallel \cdot \nabla_\parallel N_s = \nabla_\parallel \cdot (H \nabla_\parallel N_s) + 2\text{Pe} S_\perp^s. \quad (\text{S100})$$

Both functions  $\Phi_w$  and  $\Phi_p$  depend only on the Peclet number and not on the electrostatic properties of the surfaces. These functions can be obtained numerically using a solver for partial differential equations. They are represented in Fig. 5.

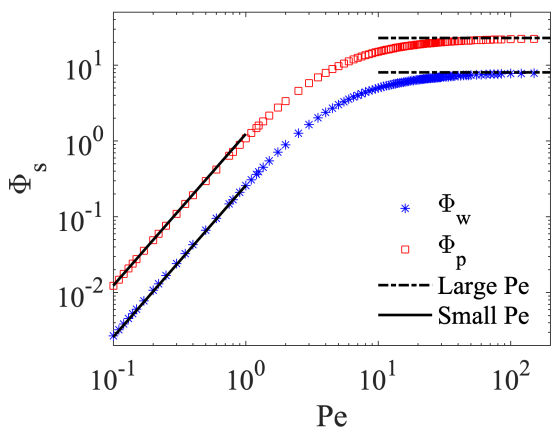


FIG. 5.  $\Phi_p$  and  $\Phi_w$  as a function of the Peclet number. Symbols are the results of the numerical integration of Eqs. (S99) and (S100). Full lines represent the retained values for small Peclet, given in Eq. (S105). Dashed lines represent the analytical results (S112) and (S113) for large Peclet numbers.

## B. Limit of small Peclet number

### 1. Case of equal zeta potentials at the particle and the wall

Analytical results can be found in the case that the wall and the surface have the same zeta potential, so that  $\alpha_w = \alpha_p \equiv \alpha$ . In this case, at small Pe, if we expand  $N$  in powers of the Peclet number as  $N \simeq N_0 + \text{Pe} N_1 + \dots$ , we readily obtain that  $N_0$  is zero, while  $N_1$  satisfies

$$H \nabla_\parallel^2 N_1 + \nabla_\parallel H \cdot \nabla_\parallel N_1 = -2\alpha(S_\perp^w + S_\perp^p), \quad (\text{S101})$$

The solution to this equation was given in Ref. [30]

$$N_1 = \frac{6\alpha X}{5H^2}. \quad (\text{S102})$$

Inserting the value of  $N \simeq \text{Pe} N_1$  into Eq. (S89), we find

$$\Phi = \frac{24\alpha^2\pi}{25} \text{Pe}^2. \quad (\text{S103})$$

This result is exactly that obtained in Ref. [30] [see equation (6.27) in this reference] for small Peclet numbers in the same conditions.

## 2. Case of distinct zeta potentials

In the case that the wall and the sphere have different electrostatic properties, we could not find analytical expressions for the force in the limit of small Peclet number. However, it is clear that one can still write  $N = \text{Pe} N_1$  for small Peclet, where  $N_1$  satisfies

$$0 = \nabla_\parallel \cdot (H \nabla_\parallel N_1) + 2(\alpha_w S_\perp^w + \alpha_p S_\perp^p). \quad (\text{S104})$$

Numerically solving for  $N_1$  leads to

$$\Phi_w \underset{\text{Pe} \rightarrow 0}{\simeq} 0.26 \text{Pe}^2, \quad \Phi_p \underset{\text{Pe} \rightarrow 0}{\simeq} 1.24 \text{Pe}^2. \quad (\text{S105})$$

Note that, with these values, one recovers Eq. (S103) when  $\alpha_p = \alpha_w$ . Interestingly, the result of Ref. [30], as given by their equation (6.27), can be written as

$$\Phi = \frac{6\pi(\alpha_p + \alpha_w)}{5} \left[ \frac{\alpha_w + \alpha_p}{5} + 1.667(\alpha_p - \alpha_w) \right] \text{Pe}^2. \quad (\text{S106})$$

This corresponds to our functional form Eq. (S98) for small Peclet, with

$$\Phi_w \underset{\text{Pe} \rightarrow 0}{\simeq} -5.53 \text{Pe}^2, \quad \Phi_p \underset{\text{Pe} \rightarrow 0}{\simeq} 7.03 \text{Pe}^2, \quad (\text{S107})$$

which differ from our results in Eq. (S105). This discrepancy may come from the fact that one of the steps in Ref. [30] consists in finding the solution to Eq. (S104), which is done by writing  $N_1$  in terms of an infinite series [see Eqs. (4.33)-(4.35) in Ref. [30]]. However, this series converges to a function that is divergent at the origin and is thus not an acceptable solution for  $N_1$ .

## C. Large Peclet numbers

In the limit of large Peclet numbers,  $N$  becomes independent on the Peclet number, and the diffusive term can be neglected in Eq. (S54) which becomes

$$\bar{\mathbf{U}}_\parallel \cdot \nabla_\parallel N = 2(\alpha_w S_\perp^w + \alpha_p S_\perp^p). \quad (\text{S108})$$

Using the expressions of the source terms and the effective flow [see Eqs (S41), (S42) and (S56)] and using polar coordinates with  $X = \rho \cos \theta$  and  $Y = \rho \sin \theta$ , we obtain

$$\begin{aligned} \frac{6 + \rho^2}{10} \cos \theta \partial_\rho N - \frac{6 + 3\rho^2}{10\rho} \sin \theta \partial_\theta N = \\ 2 \cos \theta \left[ \alpha_w \frac{16\rho(4 - \rho^2)}{5(\rho^2 + 2)^3} + \alpha_p \frac{4\rho(\rho^2 + 26)}{5(\rho^2 + 2)^3} \right]. \end{aligned} \quad (\text{S109})$$

We remark that we can find a solution  $N(\rho)$  that depends only on the radial coordinate  $\rho$ , so that

$$\partial_\rho N = 16 \frac{4\alpha_w \rho (4 - \rho^2) + \alpha_p \rho (\rho^2 + 26)}{(6 + \rho^2) (\rho^2 + 2)^3}. \quad (\text{S110})$$

Using this expression to calculate (S88), we find that the dimensionless lift force for large Peclet number reads

$$\Phi \simeq \pi(\alpha_w + \alpha_p) \left[ (64 - 45 \ln 3) \frac{\alpha_p}{2} + \alpha_w (52 - 45 \ln 3) \right]. \quad (\text{S111})$$

Equivalently, we can write the limiting values of  $\Phi_p, \Phi_w$  for large Peclet as

$$\Phi_p \underset{\text{Pe} \rightarrow \infty}{\simeq} \pi(64 - 45 \ln 3) \frac{1}{2} \simeq 22.87, \quad (\text{S112})$$

$$\Phi_w \underset{\text{Pe} \rightarrow \infty}{\simeq} \pi(52 - 45 \ln 3) \simeq 8.05. \quad (\text{S113})$$

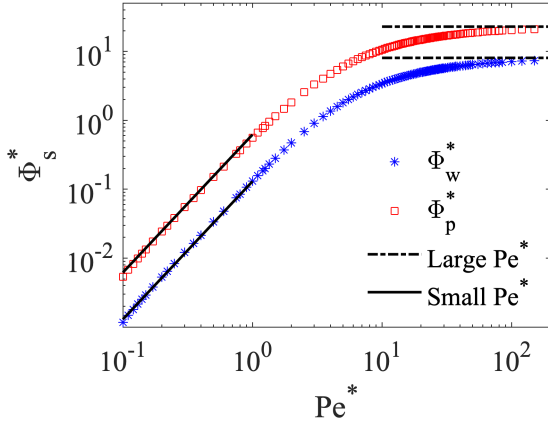


FIG. 6.  $\Phi_p^*$  and  $\Phi_w^*$  as a function of the characteristic Peclet number  $\text{Pe}^*$  in the experimentally relevant case of sinusoidal variation of the velocity. Symbols are obtained by using Eq. (S121) and the data for  $\Phi_s$  and  $\Phi_w$  shown in Fig. 5. Full lines represent the retained values for small Peclet, given in Eq. (S105), with  $\Phi_s^* \simeq \Phi_s/2$ . Dashed lines represent the analytical results Eqs. (S112) and (S113) for large Peclet numbers, where  $\Phi_s^* \simeq \Phi_s$ .

#### D. Temporally averaged force

In the experiments the velocity is not constant but is applied as a sinusoidal function:

$$V(t) = V_0 \sin(\omega t) \quad (\text{S114})$$

so that the (instantaneous) Peclet number becomes time dependent. We therefore define

$$\text{Pe}^* = V_0 \sqrt{Rd}/D_e, \quad \text{Pe}(t) = \text{Pe}^* \sin(\omega t). \quad (\text{S115})$$

If  $\omega$  is sufficiently low, the instantaneous force predicted by our theory reads

$$F_{\text{lift}} = F_0 \Phi(\text{Pe}^* \sin(\omega t)). \quad (\text{S116})$$

Here we have assumed that  $\omega$  is sufficiently low so that one can consider that the force depends only on the instantaneous velocity. The validity of this quasi-static approximation is discussed in Section V. The average force can be written as

$$\langle F_{\text{lift}} \rangle = F_0 \Phi^*(\text{Pe}^*), \quad (\text{S117})$$

where the scaling function  $\Phi^*$  reads

$$\Phi^*(\text{Pe}^*) = \frac{1}{2\pi} \int_0^{2\pi} dt \Phi(\text{Pe}^* \sin t). \quad (\text{S118})$$

In practice we may evaluate this integral on the interval  $[0, \pi/2]$  only, by using  $u = \text{Pe}^* \sin(t)$ , one obtains

$$\Phi^*(\text{Pe}^*) = \frac{2}{\pi} \int_0^{\text{Pe}^*} \frac{du}{\text{Pe}^* \sqrt{1 - \left(\frac{u}{\text{Pe}^*}\right)^2}} \Phi(u). \quad (\text{S119})$$

We may also define  $\Phi_s^*$  such that

$$\Phi^* = (\alpha_p + \alpha_w)(\Phi_w^* \alpha_w + \Phi_p^* \alpha_p), \quad (\text{S120})$$

with

$$\Phi_s^*(\text{Pe}^*) = \frac{2}{\pi} \int_0^{\text{Pe}^*} \frac{du}{\text{Pe}^* \sqrt{1 - \left(\frac{u}{\text{Pe}^*}\right)^2}} \Phi_s(u) \quad (\text{S121})$$

For small arguments,  $\Phi_s^*(u) \simeq \Phi_s(u)/2$  where the factor one half comes from the quadratic dependence with the velocity, with  $\langle \cos^2(t) \rangle = 1/2$ . At large Peclet numbers, the force does not depend on the velocity, and the functions  $\Phi$  and  $\Phi^*$  become equal. The functions  $\Phi_p^*$  and  $\Phi_w^*$  are shown in Fig. 6.

## V. DYNAMICS

Here we briefly discuss dynamic effects. To evaluate the lift force, we assumed that the lift force can be calculated at each time by using the result of the theory which assumes a stationary state under the velocity (quasi-static assumption). Here we control the validity of this assumption. The slowest varying field is the concentration because its dynamics is governed by diffusion, in comparison the electric field and the hydrodynamic flow adapt much faster to external perturbations. Hence, the only modification in the theory to take into account time dependent effects is to add a term  $\partial_t c$  in the equation for  $c$ . It is useful to use dimensionless variables, we set  $\tau = t D_e / l^2$ , and  $\Omega = \omega l^2 / D_e$ . Equation (S45) becomes

$$\varepsilon [\partial_\tau c + \text{Pe}(U_X \partial_X c + U_Y \partial_Y c + U_Z \partial_Z c)] = \partial_Z^2 c + \varepsilon \nabla_{\parallel}^2 c, \quad (\text{S122})$$

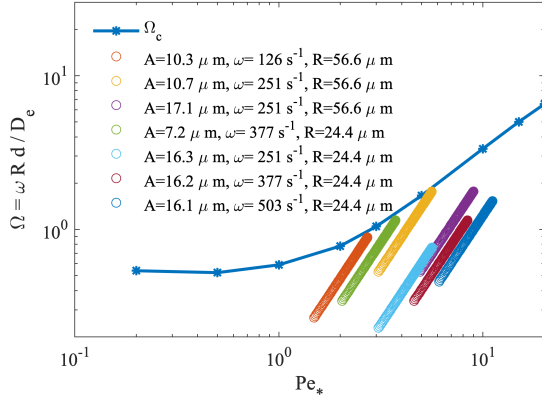


FIG. 7.  $\Omega_c$ , defined as the value of  $\Omega$  such that the average force differs by less than 15% of the force calculated with the quasi-static hypothesis if  $\Omega < \Omega_c$ . We report also the value of  $\Omega$  for the experimental parameters corresponding to the curves plotted in Fig. 4 of the main text, for distances  $d \in [60; 200]$  nm.

where  $\text{Pe}(\tau) = \text{Pe}^* \cos(\Omega\tau)$ . We still look for solutions under the form  $c = c_\infty + c_\infty \lambda^2 / d^2 (N + \varepsilon N_1 + \dots)$ , where at leading order  $N$  does not depend on  $Z$ . At next order we have

$$\partial_\tau N + \text{Pe} \mathbf{U}_\parallel \cdot \nabla_\parallel N = \partial_Z^2 N_1 + \nabla_\parallel^2 N, \quad (\text{S123})$$

Integrating over  $Z \in [0, H]$  leads to

$$\begin{aligned} H \partial_\tau N + \text{Pe}(\tau) \bar{\mathbf{U}}_\parallel \cdot \nabla_\parallel N &= \nabla_\parallel \cdot (H \nabla_\parallel N) \\ &+ 2\text{Pe}(\tau) (\alpha_w S_\perp^w + \alpha_p S_\perp^p). \end{aligned} \quad (\text{S124})$$

The instantaneous dimensionless force can then be calculated by using Eq. (S88). We have numerically solved Eq. (S124) and identified, for each value of the Peclet, the value of  $\Omega$  for which the temporally averaged force differs by 15% from the result of our theory using the quasi-static approximation. This value is reported in Fig. 7 for experimental parameters, together with the values of  $\Omega$  in all the experiments. From the fact that  $\Omega < \Omega_c$  for all experiments, we conclude that the oscillation frequency is low enough to ensure the validity of the quasi-static assumption.

---

[1] Lyklema, J. *Fundamentals of interface and colloid science: soft colloids*, vol. 5 (Elsevier, 2005).

[2] Robert J, H. *Fundamentals of colloid science* (Oxford University Press, 2001).

[3] Stone, H. A., Stroock, A. D. & Ajdari, A. Engineering flows in small devices: microfluidics toward a lab-on-a-chip. *Annu. Rev. Fluid Mech.* **36**, 381–411 (2004).

[4] Bocquet, L. & Charlaix, E. Nanofluidics, from bulk to interfaces. *Chemical Society Reviews* **39**, 1073–1095 (2010).

[5] Stein, D., Kruithof, M. & Dekker, C. Surface-charge-governed ion transport in nanofluidic channels. *Physical Review Letters* **93**, 035901 (2004).

[6] Tawari, S. L., Koch, D. L. & Cohen, C. Electrical double-layer effects on the brownian diffusivity and aggregation rate of laponite clay particles. *Journal of Colloid and Interface Science* **240**, 54–66 (2001).

[7] Eichmann, S. L., Anekal, S. G. & Bevan, M. A. Electrostatically confined nanoparticle interactions and dynamics. *Langmuir* **24**, 714–721 (2008).

[8] Horn, F., Richtering, W., Bergenholz, J., Willenbacher, N. & Wagner, N. Hydrodynamic and colloidal interactions in concentrated charge-stabilized polymer dispersions. *Journal of colloid and interface science* **225**, 166–178 (2000).

[9] Rubio-Hernández, F., Carrique, F. & Ruiz-Reina, E. The primary electroviscous effect in colloidal suspensions. *Advances in Colloid and Interface Science* **107**, 51–60 (2004).

[10] Liu, F., Klaassen, A., Zhao, C., Mugele, F. & Van Den Ende, D. Electroviscous dissipation in aqueous electrolyte films with overlapping electric double layers. *The Journal of Physical Chemistry B* **122**, 933–946 (2018).

[11] Zhao, C., Zhang, W., van den Ende, D. & Mugele, F. Electroviscous effects on the squeezing flow of thin electrolyte solution films. *Journal of fluid mechanics* **888**, A29 (2020).

[12] Rodríguez Matus, M. *et al.* Electroviscous drag on squeezing motion in sphere-plane geometry. *Physical Review E* **105**, 064606 (2022).

[13] Jin, D., Hwang, Y., Chai, L., Kampf, N. & Klein, J. Direct measurement of the viscoelectric effect in water. *Proceedings of the National Academy of Sciences* **119**, e2113690119 (2022).

[14] Cramail, C., Lhermerout, R. & Charlaix, E. Theory of hydrodynamic forces in electric double layers. *arXiv preprint arXiv:2503.23853* (2025).

[15] Alexander, B. M. & Prieve, D. C. A hydrodynamic technique for measurement of colloidal forces. *Langmuir* **3**, 788–795 (1987).

[16] Bike, S. G. & Prieve, D. C. Electrohydrodynamic lubrication with thin double layers. *Journal of colloid and interface science* **136**, 95–112 (1990).

[17] Bike, S. & Prieve, D. Electrohydrodynamics of thin double layers: a model for the streaming potential profile. *Journal of colloid and interface science* **154**, 87–96 (1992).

[18] Bike, S. & Prieve, D. Electrokinetic lift of a sphere moving in slow shear flow parallel to a wall: II. theory. *Journal of colloid and interface science* **175**, 422–434 (1995).

[19] Saintyves, B., Jules, T., Salez, T. & Mahadevan, L. Self-sustained lift and low friction via soft lubrication. *Proceedings of the National Academy of Sciences* **113**, 5847–5849 (2016).

[20] Rallabandi, B., Oppenheimer, N., Ben Zion, M. Y. & Stone, H. A. Membrane-induced hydroelastic migration of a particle surfing its own wave. *Nature Physics* **14**, 1211–1215 (2018).

[21] Davies-Strickleton, H. *et al.* Elastohydrodynamic lift at

a soft wall. *Physical review letters* **120**, 198001 (2018).

[22] Zhang, Z. *et al.* Direct measurement of the elastohydrodynamic lift force at the nanoscale. *Physical review letters* **124**, 054502 (2020).

[23] Zhang, H. *et al.* Direct measurement of the viscoelastic lift force near a liquid interface. *Physical Review Letters* **134**, 094001 (2025).

[24] Bureau, L., Coupier, G. & Salez, T. Lift at low reynolds number. *The European Physical Journal E* **46**, 111 (2023).

[25] Cox, R. Electroviscous forces on a charged particle suspended in a flowing liquid. *Journal of Fluid Mechanics* **338**, 1–34 (1997).

[26] Yariv, E., Schnitzer, O. & Frankel, I. Streaming-potential phenomena in the thin-debye-layer limit. part 1. general theory. *Journal of fluid mechanics* **685**, 306–334 (2011).

[27] Schnitzer, O., Frankel, I. & Yariv, E. Streaming-potential phenomena in the thin-debye-layer limit. part 2. moderate péclet numbers. *Journal of fluid mechanics* **704**, 109–136 (2012).

[28] Warszyński, P., Wu, X. & Van De Ven, T. Electrokinetic lift force for a charged particle moving near a charged wall—a modified theory and experiment. *Colloids and Surfaces A: Physicochemical and Engineering Aspects* **140**, 183–198 (1998).

[29] Warszyński, P. & van de Ven, T. Electroviscous forces on a charged cylinder moving near a charged wall. *Journal of Colloid and Interface Science* **223**, 1–15 (2000).

[30] Tabatabaei, S., van de Ven, T. & Rey, A. Electroviscous sphere–wall interactions. *Journal of colloid and interface science* **301**, 291–301 (2006).

[31] Tabatabaei, S., van de Ven, T. & Rey, A. Electroviscous cylinder–wall interactions. *Journal of colloid and interface science* **295**, 504–519 (2006).

[32] Bike, S., Lazarro, L. & Prieve, D. Electrokinetic lift of a sphere moving in slow shear flow parallel to a wall: I. experiment. *Journal of colloid and interface science* **175**, 411–421 (1995).

[33] Wu, X., Warszyński, P. & van de Ven, T. G. Electrokinetic lift: observations and comparisons with theories. *Journal of colloid and interface science* **180**, 61–69 (1996).

[34] Cevheri, N. & Yoda, M. Lift forces on colloidal particles in combined electroosmotic and poiseuille flow. *Langmuir* **30**, 13771–13780 (2014).

[35] Ducker, W. A., Senden, T. J. & Pashley, R. M. Direct measurement of colloidal forces using an atomic force microscope. *nature* **353**, 239–241 (1991).

[36] Butt, H.-J., Cappella, B. & Kappl, M. Force measurements with the atomic force microscope: Technique, interpretation and applications. *Surface science reports* **59**, 1–152 (2005).

[37] Craig, V. S. & Neto, C. In situ calibration of colloid probe cantilevers in force microscopy: hydrodynamic drag on a sphere approaching a wall. *Langmuir* **17**, 6018–6022 (2001).

[38] Israelachvili, J. N. *Intermolecular and surface forces* (Academic press, 2011).

[39] O’neill, M. & Stewartson, K. On the slow motion of a sphere parallel to a nearby plane wall. *Journal of Fluid Mechanics* **27**, 705–724 (1967).

[40] Jeffrey, D. & Onishi, Y. The slow motion of a cylinder next to a plane wall. *The Quarterly Journal of Mechanics and Applied Mathematics* **34**, 129–137 (1981).